Indocyanine-green-embedded PEBBLEs as a contrast agent for photoacoustic imaging

Gwangseong Kim
University of Michigan
Department of Chemistry
Ann Arbor, Michigan 48109

Sheng-Wen Huang
University of Michigan
Department of Biomedical Engineering
Ann Arbor, Michigan 48109

Kathleen C. Day
University of Michigan
Department of Urology and Comprehensive Cancer Center
Ann Arbor, Michigan 48109

Matthew O'Donnell
University of Michigan
Department of Biomedical Engineering
Ann Arbor, Michigan 48109

Rodney R. Agayan
University of Michigan
Department of Chemistry
Ann Arbor, Michigan 48109

Mark A. Day
University of Michigan
Department of Urology and Comprehensive Cancer Center
Ann Arbor, Michigan 48109

Raoul Kopelman
University of Michigan
Department of Chemistry
Ann Arbor, Michigan 48109

Shai Ashkenazi
University of Michigan
Department of Biomedical Engineering
Ann Arbor, Michigan 48109

Abstract. Nanoparticles 100 nm in diameter containing indocyanine green (ICG) have been developed as a contrast agent for photoacoustic (PA) imaging based on (photonic explorers for biomedical use by biologically localized embedding PEBBLE) technology using organically modified silicate (ormosil) as a matrix. ICG is an FDA-approved dye with strong optical absorption in the near-infrared (NIR) region, where light can penetrate deepest into biological tissue. A photoacoustic imaging system was used to study image contrast as a function of PEBBLE concentration in phantom objects. ICG-embedded ormosil PEBBLEs showed improved stability in aqueous solution compared with free ICG dye. The particles were conjugated with HER-2 antibody for breast cancer and prostate cancer cell targeting. Initial *in vitro* characterization shows high contrast and high efficiency for binding to prostate cancer cells. ICG can also be used as a photosensitizer (generating toxic oxygen by illumination) for photodynamic therapy. We have measured the photosensitization capability of ICG-embedded ormosil nanoparticles. This feature can be utilized to combine detection and therapeutic functions in a single agent. [DOI: 10.1117/1.2771530]

Keywords: photoacoustic (PA) imaging; cell targeting; photonic explorers for biomedical use by biologically localized embedding (PEBBLE); indocyanine green (ICG).

Paper 06338R received Nov. 19, 2006; revised manuscript received Mar. 29, 2007; accepted for publication Apr. 28, 2007; published online Aug. 27, 2007.

1 Introduction

Photoacoustic (PA) imaging is an emerging biomedical modality based on detecting acoustic signals generated from biological tissues by optical absorption. Pulsed laser illumination is used to induce rapid thermoelastic expansion in a tissue volume launching acoustic waves. An ultrasonic array transducer detects the acoustic radiation for image reconstruction. The image reflects the distribution of optical absorption in tissue. The technique combines the high spatial resolution and penetration of ultrasonic imaging with the high contrast related to the optical properties of tissue. PA imaging has been demonstrated for imaging blood vasculature, including functional brain visualization in a small animal,[1–3] and has been studied for detection of various types of cancer such as breast,[4] skin,[5,6] and eye[7] and diagnostics of renal diseases.[8]

Address all correspondence to: Raoul Kopelman and Shai Ashkenazi, 2200 Bonisteel Blvd., Ann Arbor, MI 48109; Tel.: 734-936-3674; Fax: 734-936-1905; E-mail: shaia@eecs.umich.edu

1083-3668/2007/12(4)/044020/8/$25.00 © 2007 SPIE

These applications are based on naturally occurring light absorbers, such as hemoglobin and melanin.

PA imaging using near-infrared (NIR) illumination in the range of 700 to 1000 nm has attracted the most attention because light can penetrate several centimeters into tissue at these wavelengths. Ideally, the tissue medium should have low optical absorption for deep penetration, while the objects of interest (such as tumors in cancer detection) should have high absorption for best image contrast. Exogenous staining can provide high contrast when the natural optical contrast is not sufficient. Several PA imaging studies utilized various NIR absorbing agents, such as indocyanine green (ICG),[9] and gold nanoparticles.[10,11]

ICG is a water-soluble, FDA-approved dye that has strong absorption around 800 nm and has been widely used for retinal angiography,[12] liver function testing,[13] and cardiac output assessment.[14] ICG can fluoresce[15] and is also a photosensitizer, that is, it generates toxic reactive oxygen by light illumination. This reaction is used in photodynamic therapy (PDT) for photoactivated chemotherapy in cancer treatment.[16–18]

We present here a dual-function, nanosize agent for both early-stage cancer detection by PA imaging and localized cancer treatment by PDT. The agent is designed by encapsulating ICG dye in a biocompatible matrix incorporating an antibody on its surface for cancer targeting. The PA imaging can be used to detect the nanoparticles without significant activation of toxic oxygen generation, because PDT light doses are typically in the range of 10 to 100 J/cm^2 (Ref. 19), which is 10^3 to 10^4 times higher than the required light fluence for a single acquisition of a photoacoustic image. An additional continuous wave (CW) laser can be used for PDT activation.

We have developed ICG-embedded nanoparticles that are incorporated with cancer-specific targeting as a contrast agent for PA imaging. The nanoparticles were developed based on PEBBLE (photonic explorers for biomedical use by biologically localized embedding) technology,[20–23] using organically modified silicate (ormosil) as the matrix.[24,25] Nanoencapsulation of ICG, has been reported for a few different applications, such as improvement/stabilization of ICG, properties, drug delivery of ICG, and photodynamic therapy.[26–29] Dye encapsulation in nanoparticles has several advantages. First, the nanoparticle surface can be engineered for specific purposes, for example, incorporation with a targeting moiety and PEGylation for extended blood circulation time.[21] Second, superior contrast is achieved by dye encapsulation because of the high concentration in the nanoparticle. Finally, encapsulation in a nanoparticle stabilizes ICG dye molecules against an aqueous media and other destabilizing effects from the biological environment.[22,26] In this paper, we describe our investigations on ICG-embedded ormosil nanoparticles for cancer-targeted photoacoustic imaging and their potential use in photodynamic therapy.

2 Material and Methods

2.1 *Materials*

Indocyanine green (ICG) and ninhydrin were purchased from Fluka, and 1,3-diphenylisobenzofuran (DPIBF), phenyltrimethoxysilane (PTMS), methyltrimethoxysilane (MTMS), aminopropyltrimethoxysilane (APTMS), ammonium hydroxide, nitric acid, and 2-iminothiolane hydrochloride (2-IT) were obtained from Aldrich. Sulfosuccinimidyl 4-[*N*-maleimidomethyl]cyclohexane-1-carboxylate (Sulfo-SMCC) was purchased from Pierce. PBS buffer was self made. Other materials used are agarose (GPG/LE, American Bioanalytical) and intralipid (Lyposin 10%, Abbott laboratories). All dyes and chemicals were used without further purification.

2.2 *ICG PEBBLE Synthesis*

ICG-embedded ormosil nanoparticles were synthesized based on a sol-gel process combined with microemulsion polymerization.[24,25,30] 80 μL of MTMS was added to 31 mL of water containing 34 μL of nitric acid. The mixture was heated to 60°C in a water bath and stirred at 1,000 RPM for 30 min on a hot plate stirrer (Signature 575, VWR International, West Chester, Pennsylvania). The reaction mixture was maintained under constant heating and stirring for 2 more hours after quick addition of 6 mL of preheated 30% ammonium hydroxide. Then, the reaction mixture was cooled to 35°C or less. 1 mL of solution containing 6 mg of ICG and 100 μL of MTMS was added to the mixture. The reaction was run for another 1 h, and 10 μL of APTMS was added to give surface amine functionality for conjugation with antibody. After 1 h, the product was filtered with a Magna nylon membrane filter (pore size 0.1 μm) with air suction. The products were resuspended in water and filtrated with an Amicon filtration system five times to remove impurities such as nonreacted monomers, dyes, and other chemicals. The resultant nanoparticles were recovered by additional suction filtration and dried under nitrogen atmosphere. Drying is necessary in order to avoid deactivation of ICG dyes in liquid environment. It also allowed us to obtain accurate particle number density information by weighing the dried powder. Morphology of the ICG ormosil PEBBLEs was characterized in the dried phase with scanning electron microscopy (XL30 FEG SEM, Philips) and in the wet phase with dynamic light scattering particle sizing (Nicomp 380/ZLS, Particle Sizing System).

The mechanism of nanoparticle formation can be described as follows: Hydrophobic monomer PTMS forms droplets in aqueous solution by fast stirring. The MTMS molecules inside the droplets are hydrolyzed in an acidic environment, from the surface of the droplets inward, resulting in homogeneous droplets with sub micrometer size. Addition of excess ammonium hydroxide highly basifies the solution, and thus, formation and growth of nanoparticles is triggered by a condensation reaction and generation of a three-dimensional (3-D) -Si-O-Si- network. To avoid deactivation of dye by heat, the reaction mixture needs to be cooled to 40°C or lower before addition of ICG. Addition of the second monomer, MTMS, helps to entrap ICG dye molecules in the network structure by making the nanoparticles more hydrophilic and forming a denser network. APTMS is used to functionalize the surface of the nanoparticle by forming primary amine groups for further surface modifications.

2.3 *PEBBLE Absorption and Dye Loading Efficiency*

To estimate ICG dye loading capacity in nanoparticles, we prepared a set of calibration samples consisting of a known

concentration of free ICG dye and blank ormosil nanoparticles. Blank particles are added to the calibration samples to match their light scattering coefficient to that of the ICG-PEBBLEs. Extinction spectra of several calibration samples with various dye concentrations were measured and compared to the extinction spectrum of the ICG-PEBBLE sample. Extinction values at 790 nm were plotted and fitted with a linear dependence on dye concentration.

2.4 *Aqueous Stability Measurement*

Solutions of 0.1 mg/mL ICG ormosil PEBBLEs in water and 1 μM free ICG dye in water were prepared. They were covered with aluminum foil and stored at room temperature for 5 days. Absorption spectra of both PEBBLE and free dye solutions were measured daily, after ultrasonication for several minutes to remove aggregation.

2.5 *Photosensitization*

The photodynamic efficacy of ICG dye has been investigated recently.[16–18] To evaluate singlet oxygen generation from ICG-embedded ormosil PEBBLEs, a singlet oxygen-sensitive chemical probe, 1,3-diphenylisobenzofuran (DPIBF) was used. DPIBF can rapidly quench singlet oxygen, reducing its fluorescence emission near 450 nm. Because of the hydrophobicity of DPIBF, the photodynamic effect was measured in an EtOH-water (50:50) mixture. A 0.1 mg/mL suspension of ICG-embedded ormosil PEBBLEs in an EtOH-water mixture and a 1 μM (concentration was arbitrarily chosen) solution of free ICG dye in an EtOH-water mixture were prepared. 0.2 mL of 10 μM DPIBF in EtOH-water solution was mixed with 2 mL of either ICG PEBBLE or free dye solution in a 4-mL capacity fluorescence quartz cuvette. The free ICG dye–or PEBBLE-DPIBF mixture was illuminated by a Ti-Sapphire laser at 800-nm wavelength with 1.4-mm beamwidth and 700-mW beam power (light fluence 1.36 kJ/cm2), in continuous wave (CW) mode, for 30 s with shaking. Fluorescence spectra of DPIBF were measured by a fluorometer in the 420 to 620 nm range, with a 412-nm excitation wavelength, before and after laser illumination.

2.6 *PEBBLE-Antibody Conjugation*

Specific binding of ICG PEBBLEs to cancer cells is achieved by conjugating HER-2 antibody (*neu* Ab-17, Labvision Corp.) onto its surface. HER-2 antibody is known to have a good affinity to breast cancer and prostate cancer cells.[31] PEBBLE-antibody conjugation was performed following three steps: attaching a cross-linker, sulfo-SMCC, on the PEBBLE surface; thiolization of the antibody; and cross-linking mediated with sulfo-SMCC between PEBBLE and the thiolized antibody. First, 2 mL of ICG-embedded amine-functionalized ormosil PEBBLE (12 mg) solution was added into 2 mL of PBS buffer (10 mM, pH 7.5) in a 20-mL scintillation vial. The solution was purged with argon and then treated with 3 mg of cross-linking agent, sulfo-SMCC (heterobifunctional, amine reactive on one side and thiol reactive on the other side). The glass vial was sealed with parafilm and covered with aluminum foil. The mixture was stirred in a 37°C water bath for 1 h. The reaction mixture was washed in a 10-mL Amicon (100 kDa filter membrane) with sodium phosphate buffer (100 mM, pH 7.2) two times. The final volume of solution was 4 mL.

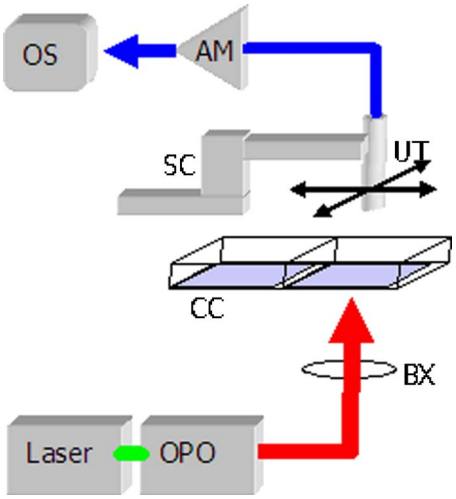

Fig. 1 A high-resolution photoacoustic scanner consisting of a doubled YAG laser, an OPO, a beam expander (BX), a sample holder (CC), a high-frequency (50 MHz) ultrasound transducer (UT), a motorized mechanical 2-D stage (SC), a signal amplifier (AM), and a digitizing oscilloscope (OS).

Second, to add a free thiol group (-SH) on the antibody available for conjugation with an SMCC attached ICG PEBBLE, the antibody was treated with 2-iminothiolane hydrochloride (2-IT). 0.1 mL of a 1 mg/mL antibody ($6.7 \cdot 10^{-7}$ mmol) solution was mixed with 2 mL of 2-IT in PBS buffer solution containing the same number of 2-IT molecules. The vial was sealed with parafilm, and the mixture was stirred at room temperature for 2 h. Finally, 4 mL of SMCC attached ICG PEBBLE solution and 2 mL of thiolized antibody solution were mixed together. This mixture was purged with argon for 1 to 2 min and stirred overnight sealed with parafilm. Then, the mixture was washed in a 10-mL Amicon filter with sodium phosphate buffer (pH 7.2) two times and with DI water three times. The washed solution was carefully transferred back to a scintillation vial and lyophilized for 3 days. The prepared antibody-conjugated ICG-ormosil PEBBLE was stored in a freezer until future use.

2.7 *Cell Targeting Efficiency of Antibody-Conjugated ICG PEBBLE*

We have tested the binding efficiency of antibodies to the PEBBLE surface and their binding to target cells. LNCaP cells, a cell line extracted from a lymph node metastasis of prostate cancer, were cultured in a cell chamber with two compartments (CultureSlides, BD Falcon™, BD BioCoat™). Cells were attached to the bottom of the chamber and their surface density was less than 50%. 0.2 mg/mL of antibody-conjugated ICG-ormosil PEBBLE and bare ICG-ormosil PEBBLE (the same batch) in PBS buffer solution were prepared and filtered with 5-μm syringe filters. They were adjusted to give similar absorption intensity at 800 nm by adding buffer solution. 1 mL of antibody-conjugated PEBBLE solution was added into one compartment, and 1 mL of unconjugated PEBBLE solution was added into the other compartment. The cell solutions were incubated for 1 h at room

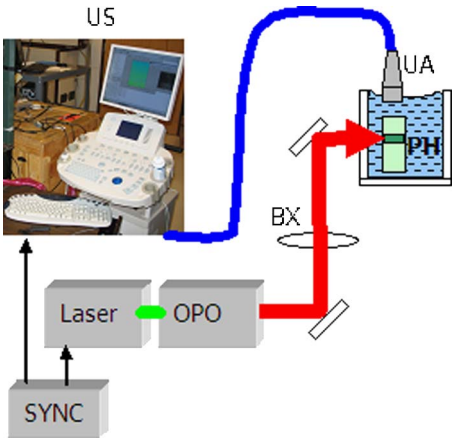

Fig. 2 Schematic of a photoacoustic imaging setup based on a clinical ultrasound scanner and a doubled YAG pulsed laser pumping an OPO. The beam is expanded (BX) before illuminating the phantom (PH). An ultrasound array probe (UA) detects the laser-generated acoustic waves. The ultrasound scanner (US) acquires signals in synchronization with the laser pulses. The scanner employs a beamforming algorithm to form the photoacoustic image.

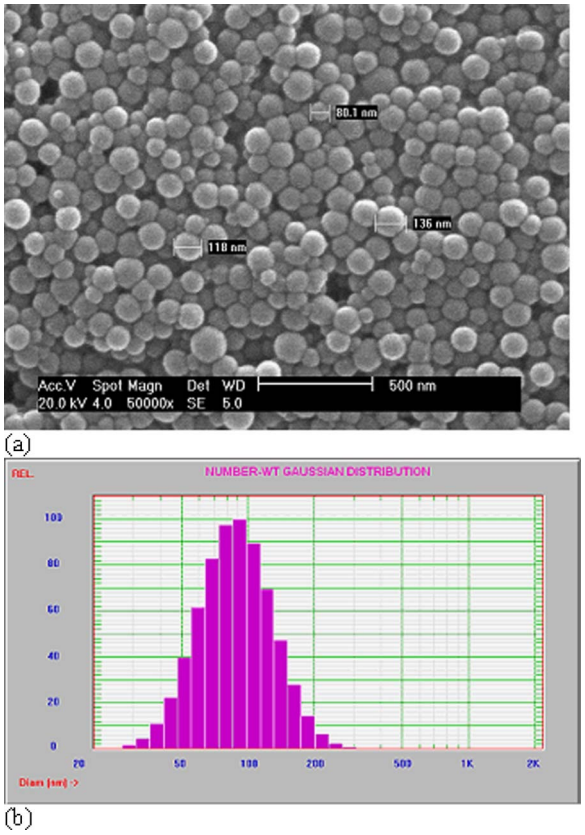

Fig. 3 (a) SEM image of ICG ormosil PEBBLE particles, and (b) particle size distribution obtained from dynamic light scattering particle sizing. (Image was taken from PEBBLE before antibody conjugation.)

temperature, and the PEBBLEs were removed from the cell chamber by washing 2 times with PBS buffer.

The efficiency of antibody targeting was confirmed by measuring the photoacoustic signal from cells treated with antibody-conjugated PEBBLE and bare PEBBLE (control). A scanning photoacoustic microscope was used to produce high-resolution images of the cells in the two compartments. The setup is shown in Fig. 1. A doubled YAG pulsed laser (Continuum, I-20) pumps an optical parametric oscillator (OPO; Continuum, Surelite OPO Plus) to produce 5-ns pulses with a tunable wavelength in the range of 690 nm to 980 nm. The output pulse energy was set to 8 mJ, and the beam diameter was expanded to 20 mm. The beam was directed to illuminate the cell chamber bottom. A single element, focused, high-frequency ultrasound transducer ($LiNbO_3$ 50 MHz, focal length=4 mm, f/1.5) detected the photoacoustic signal. The transducer focal plane was aligned with the chamber bottom surface. The transducer was mounted on a motorized XYZ translation stage to accurately scan the total volume of the cell chamber. The transducer signal is amplified (Panametrics, Model 5910PR), digitized by a digital oscilloscope (LeCroy, WaveSurfer 432), and transferred to a computer for storage. The computer was also used to control scanning.

2.8 *Photoacoustic Imaging Setup*

The scanning photoacoustic microscope described earlier is designed for imaging of tissue culture specimens. Given its limited depth of field (60 μm for the low f# transducer used) and long data acquisition time (limited by mechanical scanning), this instrument is not appropriate for clinical applications. To explore the potential of PEBBLEs for clinical applications, a second photoacoustic imaging system with lower spatial resolution but appropriate for clinical applications was developed. The system uses a clinical ultrasound scanner (Ultrasonix, Sonix RP). A software development kit, available from the scanner manufacturer, allows full control over the ultrasound beam former operation and signal acquisition hardware using C/C++ programming language. We have utilized this feature to customize the scanner for a dual-mode operation where both B-mode ultrasound and photoacoustic imaging modes are implemented. Figure 2 shows the schematic of the dual-mode imaging system.

In the photoacoustic mode, the ultrasound scanner receives the acoustic emission (generated by the pulsed laser) using a linear array ultrasound probe (Ultrasonix L-14-5/38, 128 elements, bandwidth 5 to 14 MHz). Laser pulses and ultrasound signal acquisition are synchronized using a common clock source (Agilent function generator) and a field programmable gate array (ezFPGA-C6-8 Module, Dallas Logic, Plano, Texas). The system is programmed to acquire the ultrasound signal on a single array element every laser pulse. A complete data set is acquired every 128 laser pulses (6.4 s). To reduce noise, 16 data sets are averaged before processing. A beamforming algorithm, employing coherent delay-and-sum and implemented using MATLAB (Mathworks, Inc.) code, was applied to reconstruct the photoacoustic image.[32]

The imaging system is more practical than the scanning photoacoustic microscope in three respects: electronic scanning for high frame rate; electronic focusing, providing uniform resolution; and the ability to change probes for different medical applications. We have used it to image phantoms containing small gelled ICG PEBBLE solutions embedded in optically diffusive gel (agarose 2%, intralipid 5%). The phantom was illuminated from the side while immersed in a water tank.

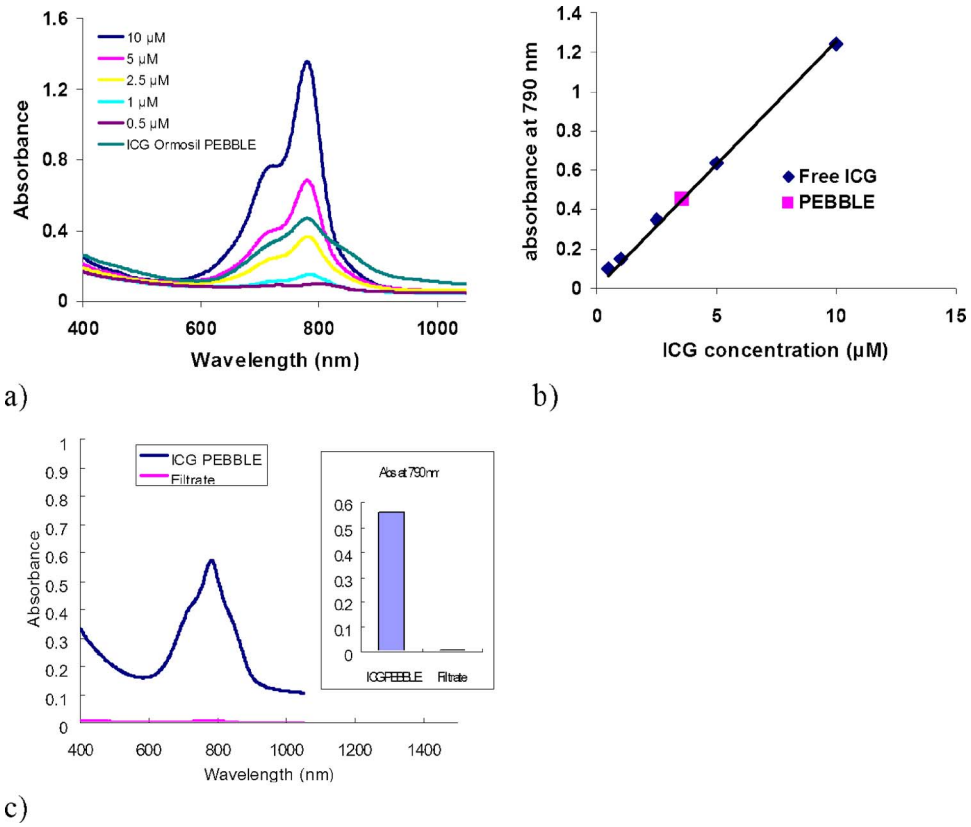

Fig. 4 (a) Dye loading in a PEBBLE particle was tested by comparing optical absorption of PEBBLE particles with optical absorption of free ICG dye at different concentrations. (b) Linear curve fitting for peak absorption (at $\lambda = 790$ nm) was evaluated to estimate the dye concentration in the PEBBLE particle. (c) Dye leaching was examined by filtration to verify that the absorption was from ICG molecules encapsulated in the PEBBLE particle.

The ultrasound transducer was positioned above the phantom.

3 Results and Discussion

3.1 *ICG PEBBLE Characterization*

ICG-embedded ormosil PEBBLEs were synthesized based on sol-gel chemistry and yielded 70 mg of nearly monodispersed nanoparticles with 100-nm diam. An SEM image of the particles (dried phase) and particle size distribution obtained from a dynamic light scattering (DLS) particle sizer (wet phase) are shown in Fig. 3. Only negligible difference in the mean particle size was observed between the dried phase and the wet phase, implying negligible swelling of particle matrix.

3.2 *PEBBLE Absorption and Dye Loading Efficiency*

Dye loading in a PEBBLE particle was tested by comparing its optical absorption with that of free ICG dye at different concentrations [see Fig. 4 (left)]. Blank ormosil particles were added to the free ICG solutions to match the scattering coefficient to that of ICG PEBBLEs. Linear curve fitting for peak absorption (at $\lambda = 790$ nm) was evaluated to estimate the dye concentration in the PEBBLE particle [Fig. 4 (right)].

The estimated dye concentration in the PEBBLE sample in 0.1 mg/mL ICG ormosil PEBBLE solution is 3.6 μM. Assuming that the density of the ormosil nanoparticle is about 2.0 g/cm^3 (Refs. 33 and 34) and considering the average particle size of 100 nm, the particle number density of 10^{11} particle/mL can be computed using the weight of particles in the solution, particle volume, and density. This dye concentration corresponds to 23,000 ICG molecules per 1 ormosil nanoparticle. High loading capacity is advantageous in cell-targeting applications. Because the number of cell-membrane receptors per area is limited, high loading per particle provides a mechanism to enhance the signal from each targeted cell.

The characteristics of the ICG PEBBLE's absorption spectrum still remain the same as that of the ICG free dye, although a minor change was observed in the reflecting interference from the ormosil matrix. According to Landsman et al.[35] and Zhou et al.,[36] at concentrations above 1 mM, ICG can forms, dimer or higher aggregated forms, resulting in a change of absorption peak shape represented by the rise of the dimer peak around 700 nm and the decline of the monomer peak at 790 nm. The shape and location of ICG PEBBLE's absorption spectrum indicates that the dye molecules are mostly present in monomer form in spite of their high packaging density in nanoparticles. In order to verify that the observed absorption spectrum corresponds to ICG molecules encapsulated in nanoparticles and is not affected by free dye in the solution due to dye leaching, the following test was performed: The PEBBLE solution was filtrated by suction using a Whatman Anodisc filtration membrane with 0.02-μm pore diameter, and absorption of the filtrate was measured. Only

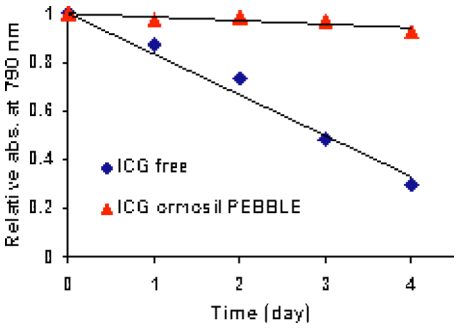

Fig. 5 Relative optical absorption of free ICG dye (diamonds) and ICG PEBBLE (triangles) measured over 5 days. Stabilization due to PEBBLE encapsulation is evident.

negligible dye leaching was observed, indicating that ICG molecules were present in monomer form in the nanoparticle. The enhanced stability of ICG in the nanoparticle is attributed to the interaction of the dye molecules with the ormosil matrix favoring monomer form by isolating individual dye molecules and preventing dye-dye interaction.

3.3 *Aqueous Stability Measurement*

The enhanced stability of ICG nanoparticles is a major advantage over free ICG dye in clinical applications. Several environmental conditions are known to affect ICG and reduce its optical absorption. Free ICG dye is unstable in aqueous media and sensitive to pH.[26,37] This instability can limit its application as an optical contrast agent in medicine. Saxena et al.[26] have reported that ICG-doped nanoparticles based on PLGA (poly latic-glycolic acid) biodegradable polymer could improve stability of ICG under the conditions described earlier. To test the stability of ICG ormosil PEBBLEs in aqueous media, we have monitored their optical absorption in a water solution for 5 days. The absorption intensity of ICG ormosil PEBBLE decreased by less than 10% over 5 days, while free ICG dye showed above 70% decrease, indicating severe deactivation in water [Fig. 5]. This result shows that encapsulation of ICG in ormosil nanoparticles improves ICG stability in aqueous media by a large factor.

3.4 *Photosensitization*

The photodynamic efficacy of ICG ormosil PEBBLEs was evaluated by monitoring the change of fluorescence intensity of a DPIBF chemical probe. DPIBF is a well-known singlet oxygen quencher with high sensitivity[38] and loses its fluorescence by reaction with singlet oxygen. As shown in Fig. 6, for laser illumination at 800 nm over 30 s, fluorescence emission of DPIBF decreased with either free ICG dye or ICG ormosil PEBBLE present. In contrast, no such decrease was observed from controls with DPIBF but without free ICG dye or ICG PEBBLEs, indicating that the decrease of DPIBF fluorescence intensity was induced by ICG. The measurement confirms the potential of ICG as a photosensitizer for PDT. The irradiated light fluence of our experiment was about 1.36 kJ/cm^2, and the PDT dose can be roughly estimated to be 2×10^{19} photons absorbed by ICG/mL, which is relatively higher than typical levels of clinical PDT. The system will be optimized for more reasonable conditions in clinical applications and the PDT efficacy of ICG ormosil PEBBLE will be investigated in more detail in our future work.

3.5 *Cell Targeting Efficiency of Antibody-Conjugated PEBBLEs*

ICG PEBBLEs were conjugated with HER-2 antibody to test targeting of prostate cancer cells (LNCaP cell line). Cells were incubated with conjugated particles and with bare particles (control) to compare specific and nonspecific binding of PEBBLEs to cells. In both cases, we used a high-resolution photoacoustic scan to detect and image a single cell layer. The scanned image of cells targeted by conjugated particles [Fig. 7(top)] has a mean signal energy 22 dB higher than that of the control cells sample [Fig. 7(bottom)], for an illumination wavelength of 800 nm. This result indicates that antibody molecules were successfully conjugated to the PEBBLEs surfaces and maintained their targeting ability. The experiment also demonstrates the potential of photoacoustic imaging for single cell detection using ICG ormosil PEBBLE cell tagging. The photoacoustic signal from cells in the control sample was higher than the noise level, indicating nonspecific binding or insufficient washing to remove all PEBBLEs. The specificity of targeting moiety will be further investigated in our future work.

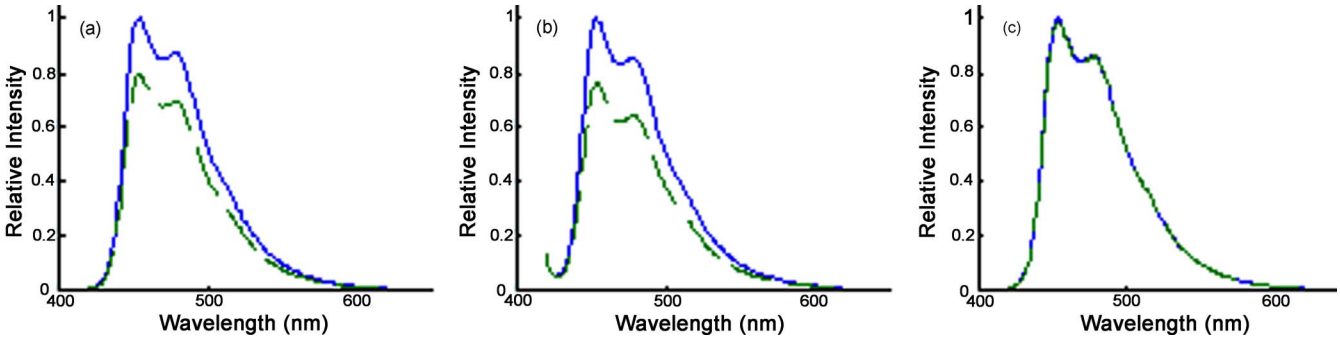

Fig. 6 (a) Fluorescence intensity of DPIBF with free ICG dye; (b) DPIBF with ICG-ormosil PEBBLEs; and (c) pure DPIBF. In each case, intensity was measured before (solid line) and after (dashed line) laser illumination at a wavelength of 800 nm for 30 s. Reduced fluorescence intensity indicates singlet oxygen generation.

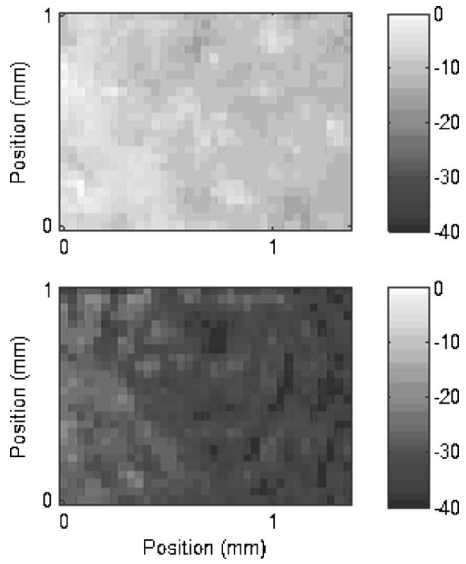

Fig. 7 Photoacoustic images of LNCaP cells incubated with antibody-conjugated PEBBLEs (top), and LNCaP cells incubated with unconjugated PEBBLEs (bottom). In both cases, cells were incubated 1 h and then washed twice. Signal gray scale is in dB.

3.6 *Photoacoustic Phantom Imaging*

We have studied the detection limits of the photoacoustic imaging setup by imaging phantom objects with inclusions of PEBBLE nanoparticles in varying concentrations. A phantom with three cylindrical inclusions, each 1.5 mm in diameter, with PEBBLE concentrations of 1 mg/mL (10^{12} PEBBLEs/cm^3), 0.1 mg/mL (10^{11} PEBBLEs/cm^3), and 0.01 mg/mL (10^{10} PEBBLEs/cm^3) were constructed. A photoacoustic image was acquired using a laser pulse energy of 12 mJ, a beamwidth of 25 mm (light fluence is 2.6 mJ/cm^2), and an illumination wavelength of 800 nm. The photoacoustic image of the phantom is shown in Fig. 8. The result showed that the PA signal intensity is clearly correlated with the PEBBLE concentration in the inclusions. The instrumental detection limit of ICG PEBBLEs for the current conditions is estimated to be about 0.01 mg/mL (10^{10} PEBBLEs/cm^3), which is equivalent to 0.36 μM of free ICG dye based on particle density calculation and the calibration curve in Sec. 3.2. At this concentration, the absorption coefficient is 0.1 cm^{-1}, which is lower than the absorption coefficient of typical tissue. For example, a recent study on the optical properties of the human prostate gland shows a mean absorption coefficient of 0.23 cm^{-1} with intersubject and intrasubject (different locations within the prostate gland) variations on the order of 0.2 cm^{-1} (Ref. 39). In this case, the minimal concentration required to provide sufficient contrast (estimated as 4 times the mean tissue background) is about 10^{11} PEBBLEs/cm^3.

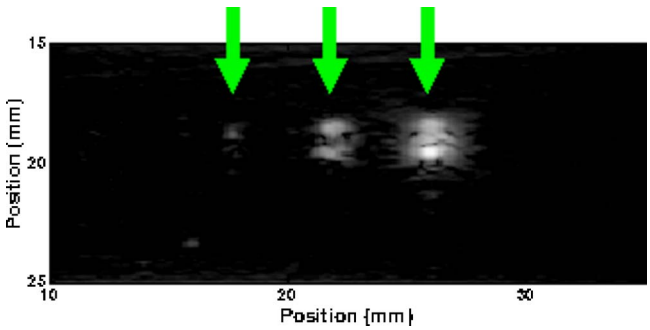

Fig. 8 Photoacoustic image of a gel phantom with three, 1.5 mm diameter, cylinders of different PEBBLE concentrations: $1\cdot10^{10}$ (PEBBLEs/cm^3) (left), $1\cdot10^{11}$ (PEBBLEs/cm^3) (middle), and $1\cdot10^{12}$ (PEBBLEs/cm^3) (right). The dynamic range of the gray scale is 40 dB.

4 Conclusion

A new type of nanoparticle for combined photoacoustic imaging and photodynamic therapy was studied. The contrast agent is based on sol-gel (ormosil) nanoparticles 100 nm in diameter, encapsulating a high concentration of ICG dye. These particles provide efficient signal enhancement for photoacoustic imaging. Based on a photoacoustic imaging system appropriate for potential clinical applications, the instrumental detection limit was determined to be 10^{10} PEBBLEs/cm^3 at an illumination intensity of only 2.6 mJ/cm^2 and a diagnostically relevant wavelength of 800 nm. To provide sufficient contrast in tissue, at least a 10 times higher concentration is required. For typical cells 20 μm in extent, this estimation corresponds to a concentration of 400 particles per cell, which is not excessive, representing an exciting prospect for molecular imaging in clinically relevant applications.

A targeting antibody (anti-Her-2/*neu*) was conjugated to the surface of the nanoparticles. Specific binding of these nanoparticles to prostate cancer cells was demonstrated *in vitro*. Targeted cells were imaged by a high-resolution photoacoustic scanner. High contrast was observed between targeted cells and nontargeted cells.

ICG PEBBLEs combine several features that make them especially attractive for future applications in cancer detection and treatment. They provide high contrast for photoacoustic imaging, can be designed easily to target specific cell membrane receptors, and can be used to generate reactive oxygen for PDT. Typical applications include prostate cancer, bladder cancer, and cancers in the gastrointestinal tract.

Acknowledgments

We thank Dr. Yong Eun Koo and Dr. Wenzhe Fan for helpful discussion and NCI Contract NO-1-CO-37123 (Kopelman) for partial support. We would also like to acknowledge the very helpful comments of the two anonymous reviewers.

References

1. R. I. Siphanto, K. K. Thumma, R. G. M. Kolkman, T. G. van Leeuwen, F. F. M. de Mul, J. W. van Neck, L. N. A. van Adrichem, and W. SteenbergenSerial, "Noninvasive photoacoustic imaging of neovascularization in tumor angiogenesis," *Opt. Express* **13**(1), 89–95 (2005).
2. X. Wang, X. Xie, G. Ku, L. V. Wang, and G. Stoica, "Noninvasive imaging of hemoglobin concentration and oxygenation in the rat brain using high-resolution photoacoustic tomography," *J. Biomed. Opt.* **11**, 024015 (2006).
3. X. Wang, G. Ku, M. A. Wegiel, D. J. Bornhop, G. Stoica, and L. V. Wang, "Noninvasive photoacoustic angiography of animal brains *in vivo* with near-infrared light and an optical contrast agent," *Opt. Lett.* **29**(7), 730–732 (2004).
4. R. O. Esenaliev, A. A. Karabutov, F. K. Tittel, B. D. Fornage, S. L. Thomsen, C. Stelling, and A. A. Oraevsky, "Laser optoacoustic im-

aging for breast cancer diagnostics: limit of detection and comparison with x-ray and ultrasound imaging," *Proc. SPIE* **2979**, 71 (1997).
5. J. A. Viator, L. O. Svaasand, G. Aguilar, B. Choi, and J. S. Nelson, "Photoacoustic measurement of epidermal melanin," *Proc. SPIE* **4960**, 14 (2003).
6. P. C. B. Rompe, F. H. dos Anjos, A. A. Martin, A. M. Mansanares, E. C. da Silva, D. Acosta-Avalos, and P. R. Barja, "Characterization of human skin through photoacoustic spectroscopy," *Proc. SPIE* **5325**, 136 (2004).
7. U. Oberheide, B. Jansen, I. Bruder, H. Lubatschowski, H. Welling, and W. Ertmer, "Optoacoustic imaging for ophthalmology," *Proc. SPIE* **4434**, 1 (2001).
8. B. Liu, V. H. Gattone II, R. A. Kruger, and K. M. Stantz, "Assessment of photoacoustic computed tomography to classify tissue in a polycystic-kidney disease mouse model," *Proc. SPIE* **6086**, 608607 (2006).
9. K. M. Stantz, B. Liu, M. Cao, D. Reinecke, K. Miller, and Robert Kruger, "Photoacoustic spectroscopic imaging of intra-tumor heterogeneity and molecular identification," *Proc. SPIE* **6086**, 608605 (2006).
10. P.-C. Li, C.-W. Wei, C.-K. Liao, C.-D. Chen, K.-C. Pao, C.-R. C. Wang, Y.-N. Wu, and D.-B. Shieh, "Multiple targeting in photoacoustic imaging using bioconjugated gold nanorods," *Proc. SPIE* **6086**, 60860M (2006).
11. A. Conjusteau, S. A. Ermilov, D. Lapotko, H. Liao, J. Hafner, M. Eghtedari, M. Motamedi, N. Kotov, and A. A. Oraevsky, "Metallic nanoparticles as optoacoustic contrast agents for medical imaging," *Proc. SPIE* **6086**, 60860K (2006).
12. W. R. Freeman, D. U. Bartsch, A. J. Mueller, A. S. Banker, and R. N. Weinreb, "Simultaneous indocyanine green and fluorescein angiography using a confocal scanning laser ophthalmoscope," *Arch. Ophthalmol. (Chicago)* **116**, 455–463 (1998).
13. T. Nonami, A. Nakao, T. Kurokawa, H. Inagaki, Y. Matsushita, J. Sakamoto, and H. Takagi, "Blood loss and ICG clearance as best prognostic markers of post-hepatectomy liver failure," *Hepato-Gastroenterology* **46**(27), 1669 (1999).
14. T. Iijima, T. Aoyagi, Y. Iwao, J. Masuda, M. Fuse, N. Kobayashi, and H. Sankawa, "Cardiac output and circulating blood volume analysis by pulse dye-densitometry," *J. Clin. Monit Comput.* **13**(2), 81–89 (1997).
15. R. C. Benson and H. A. Kues, "Fluorescence properties of Indocyanine Green as related with angiography," *Phys. Med. Biol.* **23**(1), 159–163 (1978).
16. S. Fickweiler, R. Szeimies, W. Bäumler, P. Steinbach, S. Karrer, A. E. Goetz, C. Abels, S. Hofstädter, and M. Lanthaler, "Indocyanine Green: intracellular uptake and phototherapeutic effects *in vitro*," *J. Photochem. Photobiol., B* **38**(2–3), 178–183 (1997).
17. L. Varriale, E. Crescenzi, V. Paba, B. Mazziotti di Celso, and G. Palumbo, "Selective light-induced modulation of Bcl-XL and Bax expressions in Indocyanine Green–loaded U937 cells: effects of continuous or intermittent photo-sensitization with low IR-light using a 805-nm diode laser," *J. Photochem. Photobiol., B* **57**(1), 66–75 (2000).
18. C. Ables, "Targeting of the vascular system of solid tumours by photodynamic therapy (PDT)," *Photochem. Photobiol. Sci.* **3**, 765–771 (2004).
19. J. H. Pinthus, A. Bogaards, R. Weersink, B. C. Wilson, and J. Trachtenberg, "Photodynamic therapy for urological malignancies: past to current approaches," *J. Urol. (Baltimore)* **175**(4), 1201–1207 (2006).
20. H. A. Clark, S. L. R. Barker, M. Brasuel, M. T. Miller, E. Monson, S. Parus, Z. Shi, A. Song, B. Thorsrud, R. Kopelman, A. Ade, W. Meixner, B. Athey, M. Hoyer, D. Hill, R. Lightle, and M. A. Philbert, "Subcellular optochemical nanobiosensors: probes encalsulated by biologically localized embedding (PEBBLEs)," *Sens. Actuators B* **51**(1–3), 12–16 (1998).
21. R. Kopelman, H. Xu, F. Yan, E. Monson, W. Tang, R. Schneider, and M. Philbert, "Preparation and characterization of poly (ethylene glycol)-coated Stöber silica nanoparticles for biomedical applications," *Proc. SPIE* **4626**, 383–393 (2002).
22. E. Monson, M. Brasuel, M. Philbert, and R. Kopelman, "PEBBLE nanosensors for *in vitro* bioanalysis," Chapter 59 in *Biomedical Photonics Handbook*, T. Vo-Dinh, Ed., pp. 1–14, CRC Press (2003).
23. H. Xu, S. M. Buck, R. Kopelman, M. A. Philbert, M. Brasuel, B. D. Ross, and A. Rehemtulla, "Photoexcitation-based nano-explorers: chemical analysis inside live cells and photodynamic therapy," *Isr. J. Chem.* **44**(1–3), 317–337 (2004).
24. Y. L. Koo, Y. Cao, R. Kopelman, S. M. Koo, M. Brasuel, and M. A. Philbert, "Real-time measurements of dissolved oxygen inside live cells by organically modified silicate fluorescent nanosensors," *Anal. Chem.* **76**(9), 2498–2505 (2004).
25. Y. Cao, Y. L. Koo, S. M. Koo, and R. Kopelman, "Ratiometric singlet oxygen nano-optodes and their use for monitoring photodynamic therapy nanoplatforms," *Photochem. Photobiol.* **81**(6), 1489–1498 (2005).
26. V. Saxena, M. Sadoqi, and J. Shao, "Enhanced photo-stability, thermal stability, and aqueous stability, of Indocyanine Green in polymeric nanoparticulate systems," *J. Photochem. Photobiol., B* **74**, 29–38 (2004).
27. V. Saxena, M. Sadoqi, and J. Shao, "Indocyanine Green–loaded biodegradable nanoparticles: preparation, physiochemical characterization, and *in vitro* release," *Int. J. Pharm.* **278**(2), 293–301 (2004).
28. V. Saxena, M. Sadoqi, and J. Shao, "Polymeric nanoparticulate delivery system for Indocyanine Green: biodistribution in healthy mice," *Int. J. Pharm.* **308**(1–2), 200–204 (2006).
29. A. J. Gomes, L. O. Lunardi, J. M. Marchetti, C. N. Lunardi, and A. C. Tedesco, "Indocyanine Green nanoparticles useful for photomedicine," *Photomed. Laser Surg.* **24**(4), 514–521 (2006).
30. H. J. Hah, J. S. Kim, B. J. Jeon, S. M. Koo, and Y. E. Lee, "Simple preparation of monodisperse hollow silica particles without using templates," *Chem. Commun. (Cambridge)* **14**, 1712–1713 (2003).
31. M. J. van de Vijver, J. L. Peterse, W. J. Mooi, P. Wisman, J. Lomans, O. Dalesio, and R. Nusse, "*Neu*-protein overexpression in breast cancer: association with comedo-type ductal carcinoma *in situ* and limited prognostic value in stage II breast cancer," *N. Engl. J. Med.* **319**(19), 1239–1245 (1988).
32. M. Xu, Y. Xu, and L. V. Wang, "Time-domain reconstruction algorithms and numerical simulations for thermoacoustic tomography in various geometries," *IEEE Trans. Biomed. Eng.* **50**(9), 1086–1099 (2003).
33. B. Fei, H. Lu, R. H. Wang, and J. H. Xin, "Monodisperse organosilica microcapsules with functional groups by self-catalysis," *Chem. Lett.* **35**(6), 622–623 (2006).
34. A. van Blaaderen and A. Vrij, "Synthesis and characterization of monodisperse colloidal organo-silica spheres," *J. Colloid Interface Sci.* **156**, 1–18 (1993).
35. M. L. J. Landsman, G. Kwant, G. A. Mook, and W. G. Zijlstra, "Light-absorbing properties, stability, and spectral stabilization of Indocyanine Green," *J. Appl. Physiol.* **40**, 575–583 (1976).
36. J. F. Zhou, M. P. Chin, and S. A. Schafer, "Aggregation and degradation of Indocyanine Green," *Proc. SPIE* **2128**, 495–505 (1994).
37. V. Saxena, M. Sadoqi, and J. Shao, "Degradation kinetics of Indocyanine Green in aqueous solution," *J. Pharm. Sci.* **92**, 2090–2097 (2003).
38. Y. Usui, M. Tsukada, and H. Nakamura, "Kinetic studies of photosensitized oxygenation by singlet oxygen in aqueous micellar solutions," *Bull. Chem. Soc. Jpn.* **51**(2), 379–384 (1978).
39. T. C. Zhu, A. Dimofte, J. C. Finlay, D. Stripp, T. Busch, J. Miles, R. Whittington, S. B. Malkowicz, Z. Tochner, E. Glatstein, and S. M. Hahn, "Optical properties of human prostate at 732 nm measured *in vivo* during motexafin lutetium–mediated photodynamic therapy," *Photochem. Photobiol.* **81**, 96–105 (2005).